Electronic Supplementary Information

Three-dimensional strain engineering in epitaxial vertically aligned nanocomposite thin films with tunable magnetotransport properties

*Xing Sun, Jijie Huang, Jie Jian, Meng Fan, Han Wang, Qiang Li, Judith L. MacManus-Driscoll, Ping Lu, Xinghang Zhang, and Haiyan Wang**

X. Sun, J. Huang, J. Jian, M. Fan, H. Wang, Q. Li, Prof. X. Zhang, Prof. H. Wang
School of Materials Engineering
Purdue University
West Lafayette, IN 47907, USA
E-mail: hwang00@purdue.edu

Prof. J. L. MacManus-Driscoll
Department of Materials Science and Metallurgy
University of Cambridge
Cambridge, CB3 OFS, U.K.

Prof. P. Lu
Sandia National Laboratories
Albuquerque, NM 87185, USA

Table S1. Synthesis condition for 3D framed thin films with pure CeO_2 as interlayer

Sample NO.	LSMO-CeO_2	CeO_2	LSMO-CeO_2	CeO_2	LSMO-CeO_2	CeO_2	LSMO-CeO_2
C0	2400	0	0	0	0	0	0
C1	1200	120	1200	0	0	0	0
C2	800	120	800	120	800	0	0
C3	600	120	600	120	600	120	600

Table S2. Synthesis condition for 3D framed thin films with pure LSMO as interlayer

Sample NO.	LSMO-CeO_2	LSMO	LSMO-CeO_2	LSMO	LSMO-CeO_2	LSMO	LSMO-CeO_2
L0	2400	0	0	0	0	0	0
L1	1200	120	1200	0	0	0	0
L2	800	120	800	120	800	0	0
L3	600	120	600	120	600	120	600

Table S3. Out-of-plane d-spacing variation of 3D framed thin films with different CeO_2

interlayers						
Sample name	CeO_2 (004) – Peak 1	error	CeO_2 (004) – Peak 2	error	LSMO (003)	error
C0	1.371875	0.000575	1.371875	0.000575	1.292525	0.000188746
C1	1.376825	0.000312	1.3688	0.000187	1.290725	0.000271953
C2	1.377825	0.000239	1.364925	0.000155	1.2889	0.000339116
C3	1.385075	0.000411	1.3631.4	0.000351	1.28785	0.000490748

Table S4. Strain variation of sample C0-C3

Sample name	Strain on CeO_2 (004) – peak 1/ (%)	Strain on CeO_2 (004) – peak 2/ (%)	Strain on LSMO (003)/ (%)
C0	0	0	0
C1	0.361	-0.224	-0.139
C2	0.434	-0.507	-0.280
C3	0.962	-0.618	-0.362

Table S5. Out-of-plane d-spacing variation of 3D framed films L0-L3with different LSMO interlayers				
Sample name	CeO_2 (004)	error	LSMO (003)	error
L0	1.37188	5.75E-4	1.29252	1.88746E-4
L1	1.37090	3.80789E-4	1.29135	2.75379E-4
L2	1.36975	3.22749E-4	1.29170	7.07107E-5
L3	1.36853	4.97284E-4	1.29185	3.88909E-4

Table S6. Strain variation of sample L0-L3		
	Strain on CeO_2 (004) / (%)	Strain on LSMO (003)/ (%)
L0	0	0
L1	-0.0711	-0.0909
L2	-0.155	-0.0638
L3	-0.244	-0.0522

The d_{00l}-spacing is calculated according to the corresponding peak position and Bragg's law $2d\sin\theta = n\lambda$. Each of nanocomposite thin film C0-C3 and L0-L3 was measured for three times to collect sufficient XRD 2θ-ω patterns for calculating the average of each d_{00l}-spacing and standard error listed in Table S3 and S5. The out-of-plane (OP) strain ε_{OP} is calculated as follows:

$$\varepsilon_{OP}(\%) = \frac{d_{00l}(3D\ framed\ thin\ film) - d_{00l}(Single\ layer\ VAN\ thin\ film\ C0)}{d_{00l}(Single\ layer\ VAN\ thin\ film\ C0)} \times 100$$

Here, d_{00l}(3D framed thin film) represents the d-spacing value of LSMO or CeO_2 phase in the 3D framed thin films C1-C3 and L1-L3; d_{00l}(Single layer VAN thin film C0) is the d-spacing value of the single layer VAN thin film C0 or L0.

For example, the out-of-plane strain ε_{OP} of LSMO phase in sample C1 is calculated as:

$$\varepsilon_{OP}(\%) = \frac{d_{LSMO(003)}(C1) - d_{LSMO(003)}(C0)}{d_{LSMO(003)}(C0)} \times 100 = \frac{1.290725 - 1.292525}{1.292525} \times 100 \cong -0.139\%$$

The current in-plane lattice parameter a' or b' is calculated according to the out-of-plane lattice parameter c':

$$a' = b' = \sqrt{\frac{V}{c'}} = \sqrt{\frac{a^3}{c'}}$$

Here V represents the volume of the unit cell, and a is the bulk lattice parameter (i.e., a_{LSMO} = 3.870 Å, a_{STO} = 3.905 Å a_{CeO2} = 5.411 Å).

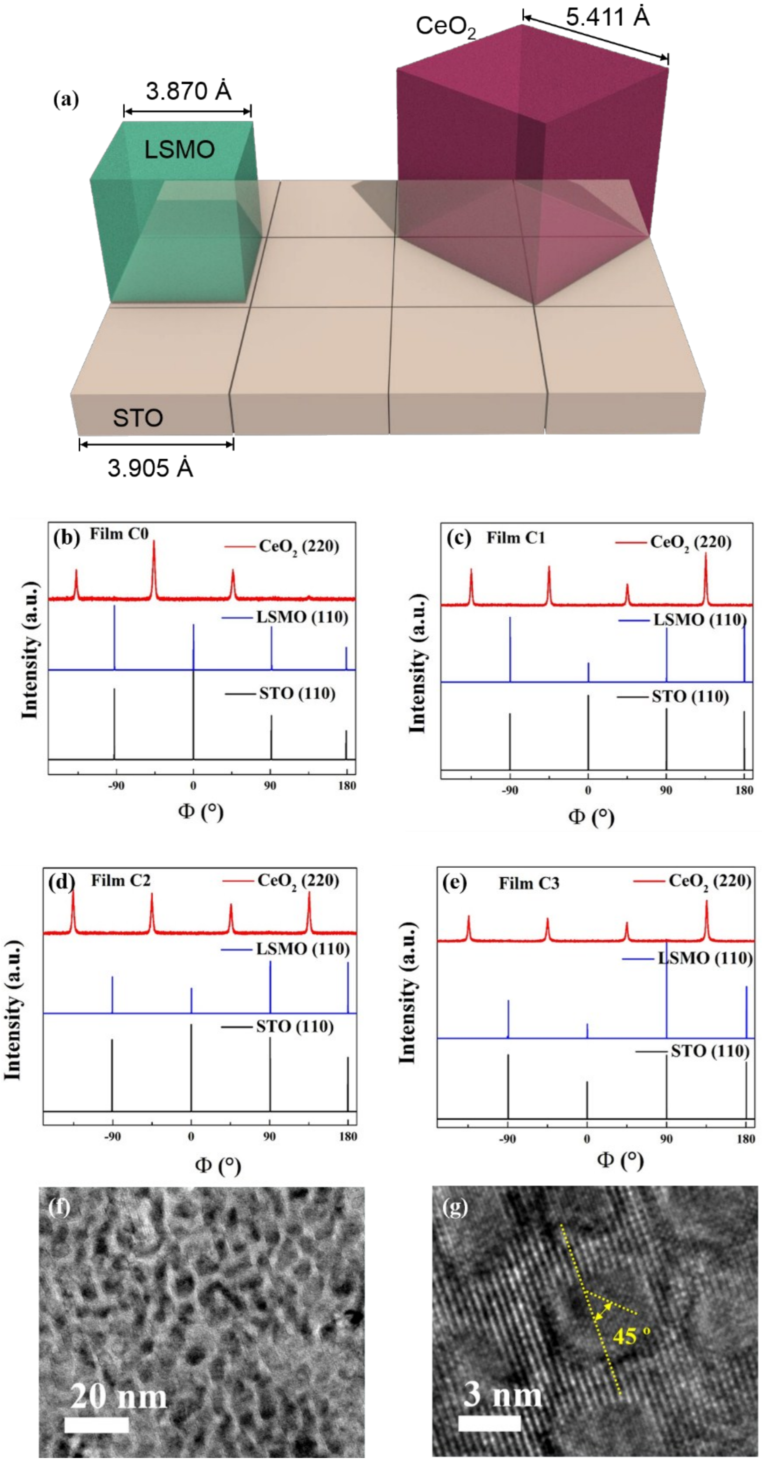

Figure S1. (a) Schematic illustration of in-plane lattice matching relations of STO(100) // CeO_2(110) and STO(100) // LSMO(100).[1-3] (b-e) ϕ scan patterns of sample C0-C3, and plan-view TEM images of sample C0 at (f) low and (g) high magnifications.

Figure S1a present the lattice matching relations between two film phases with substrate STO: CeO_2 is in a well in-plane lattice matching with STO substrate after 45º in-plane rotation; while LSMO was stacked on STO substrate in a cube-on-cube fashion without rotation. Those lattice matching relations of STO(100) // CeO_2(110) and STO(100) // LSMO(100) are confirmed by ϕ scan patterns of all 3D framed thin films C0-C3 in **Figure S1**b-e, respectively. Four-peak structure demonstrates the in-plane "cube-on-cube" stacking pattern of LSMO growing epitaxially on STO (001) substrate in all sample C0-C3. 45º in-plane rotation is determined to exist between CeO_2 and STO / LSMO from CeO_2(220) // STO (110) and CeO_2(220) // LSMO(110) in sample C0-C3. Non-equal intensity of the peaks in ϕ scans suggests a difference between the in-plane *a*- and *b*- lattice parameters. Meanwhile, it is directly observed a 45º in-plane rotation between LSMO and CeO_2 phases in plan-view HRTEM of C0 (**Figure S1**g). Due to these lattice matching relations and the bulk lattice parameter relation of $a_{CeO2}/\sqrt{2} < a_{LSMO} < a_{STO}$ ($a_{CeO2}/\sqrt{2} = 3.826$ Å, $a_{LSMO} = 3.870$ Å, $a_{STO} = 3.905$ Å), the insertion of the lateral CeO_2 interlayers reduces the in-plane d-spacing and further increases out-of-plane d-spacing of the vertical CeO_2 nanopillars in the 3D interconnected CeO_2 frameworks. It explains the interesting phenomena that the d_{00l}-spacing of the vertical CeO_2 nanopillars is gradually exaggerated from C0 to C3 solely by insertion of lateral CeO_2 interlayers in Fig. 3d.[1-3]

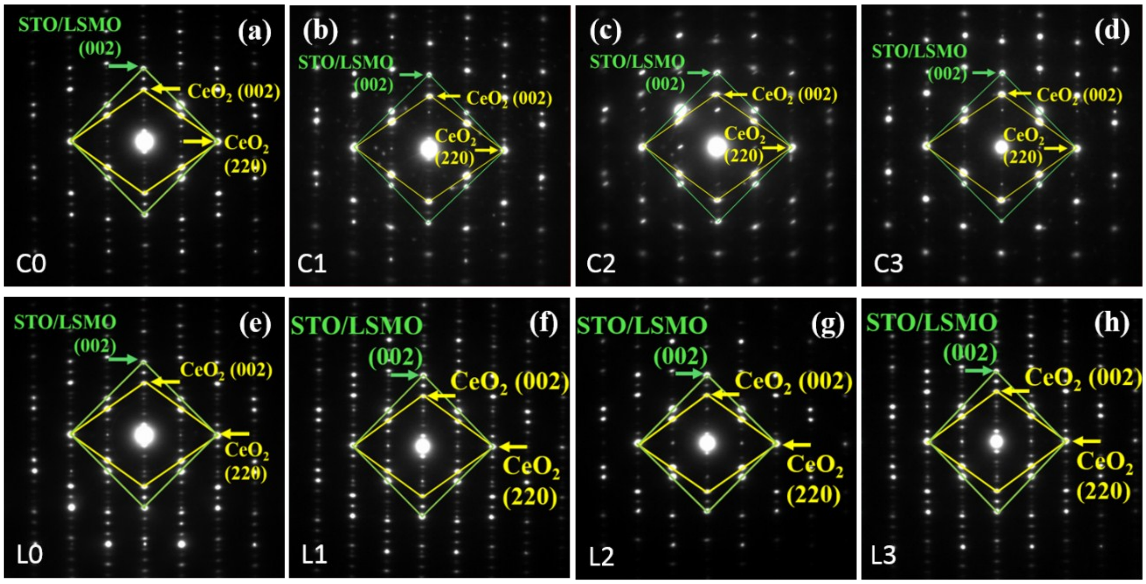

Figure S2. Cross-section selected-area electron diffraction (SAED) patterns of the 3D framed thin films with different interlayers: (a-d) C0-C3 embedding 0-3 horizontal CeO_2 interlayers and (e-h) L0-L3 with 0-3 LSMO interlayers, respectively. Those SAED patterns correspond to the cross-section TEM images in **Figure 2**.

High epitaxial growth quality in all as-prepared sample C0-C3 and L1-L3 is revealed from well-defined distinct diffraction dots in those selected area electron diffraction (SAED) patterns (**Figure S2**). No phase transition is observed in LSMO or CeO_2 phases during the strain modulation. Epitaxial correlations between films and substrates are confirmed to be CeO_2(002) || LSMO(002) || STO(002) and CeO_2[220] || LSMO[200] || STO[200]. The SAED results keep high consistence with XRD ϕ scan data.

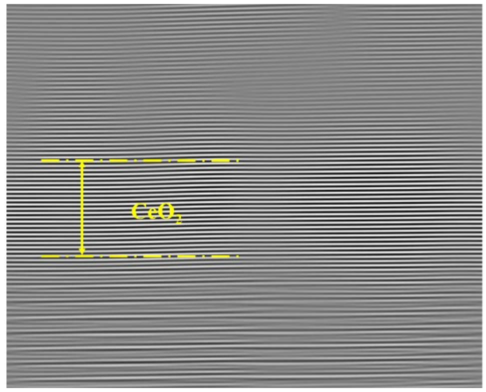

Figure S3. The fast-Fourier filtered image of **Figure 4**b.

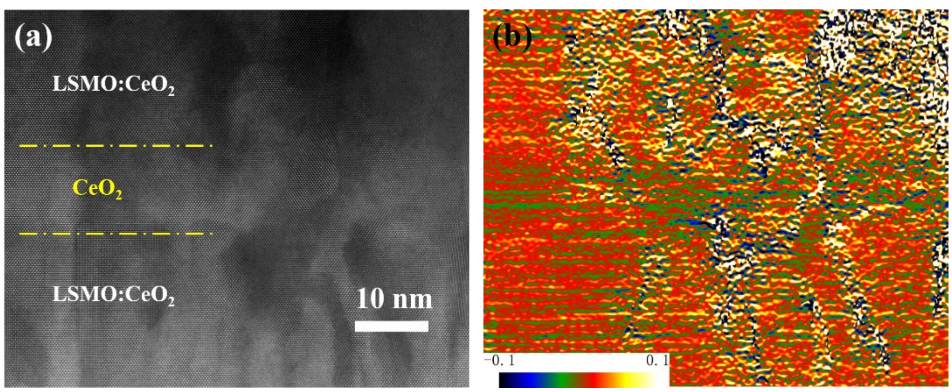

Figure S4. (a) HRSTEM image of C3 at the second CeO_2 interlayer (marked as 2 in Figure 4d), and (b) its corresponding GPA ε_{yy} (out-of-plane strain) map.

Figure S4a shows HRSTEM image of the second lateral CeO_2 interlayer of sample C3, corresponding to the area marked as 2 in **Figure 4**d. As mentioned before, 45∘ in-plane rotation interrupts the ordered arrangement in nanocomposite films. Strain distribution around this second lateral CeO_2 interlayer is also influenced and not well-defined.

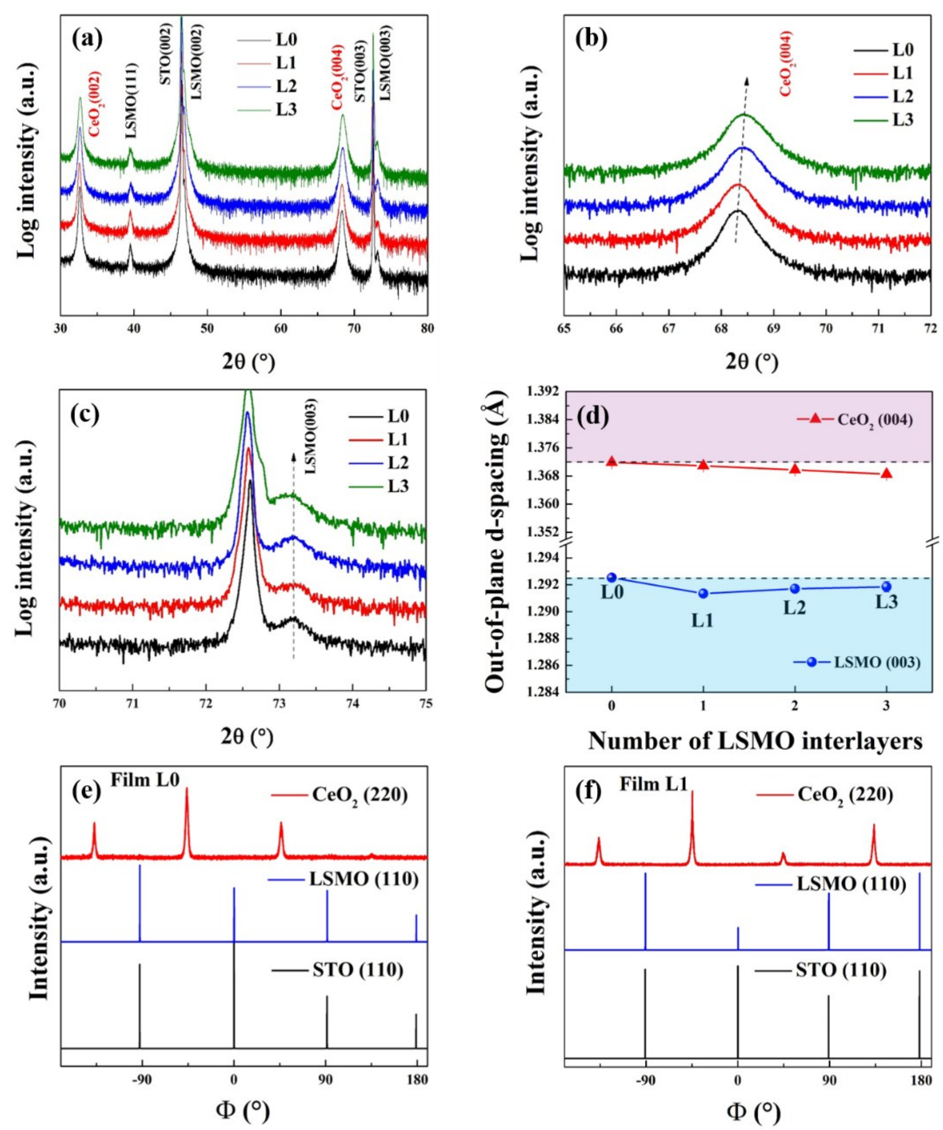

Figure S5. (a) XRD 2θ-ω patterns of the VAN thin film L0 and the 3D LSMO framed thin films L1-L3. (b) Local CeO_2 (004) 2θ-ω scans of the VAN thin film L0 and the 3D LSMO framed thin films L1-L3. (c) Local LSMO (003) 2θ-ω scans of the VAN thin film L0 and the 3D LSMO framed thin films L1-L3. (d) Systematic tuning out-of-plane d-spacing of CeO_2 (004) and LSMO (003) by 3D structure engineering in L0-L3 (the error bars are shown according to Table S5). The pink region on the top represents out-of-plane tensile strain area of CeO_2 phase and blue region on the bottom represents out-of-plane compressive strain area of LSMO phase, compared to sample L0. ϕ scan patterns of (e) L0 and (f) L1 films along (110) direction.

The 3D LSMO frameworks are constructed in Samples L1-L3 by inserting 1-3 lateral LSMO interlayers into the LSMO-CeO_2 VAN thin film L0 as shown in Fig. 1 and 2. Similarly, XRD 2θ-ω patterns in Fig. S5a demonstrate that all the thin films L0-L3 grow highly textured along (00l) direction on STO (001) substrates. LSMO and CeO_2 grow separately without apparent intermixing in the thin films L0-L3. With the increasing number of the lateral LSMO interlayers, CeO_2 (004) peaks gradually shift to higher angles (Fig. S5b), implying the slightly reduced $d_{CeO2(004)}$-spacing from L0 to L3. The LSMO (003) peaks in L0-L3 remain relatively constant as the lateral LSMO interlayers increase (Fig. S5c), revealing similar $d_{LSMO(003)}$-spacing in L0-L3. According to Table S5, the out-of-plane d-spacing variations of CeO_2 (004) and LSMO (003) in L0-L3 are plotted in Fig. S5d. Compared to sample C0, the CeO_2 vertical nanopillars are under minor compressive strain out-of-plane in L1-L3 under the effects of the 3D LSMO frameworks. The out-of-plane d-spacing of LSMO matrix basically remains the same. Therefore, the strain tunability out-of-plane is dominated by the 3D interconnected LSMO frames in L1-L3 with minimal impacts on the out-of-plane strain coupling between LSMO matrix and CeO_2 vertical nanopillars.

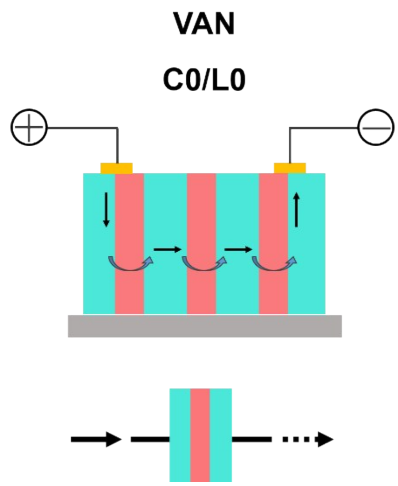

Figure S6. Schematic illustration of circuit model for VAN structured C0 without lateral CeO_2 interlayer.

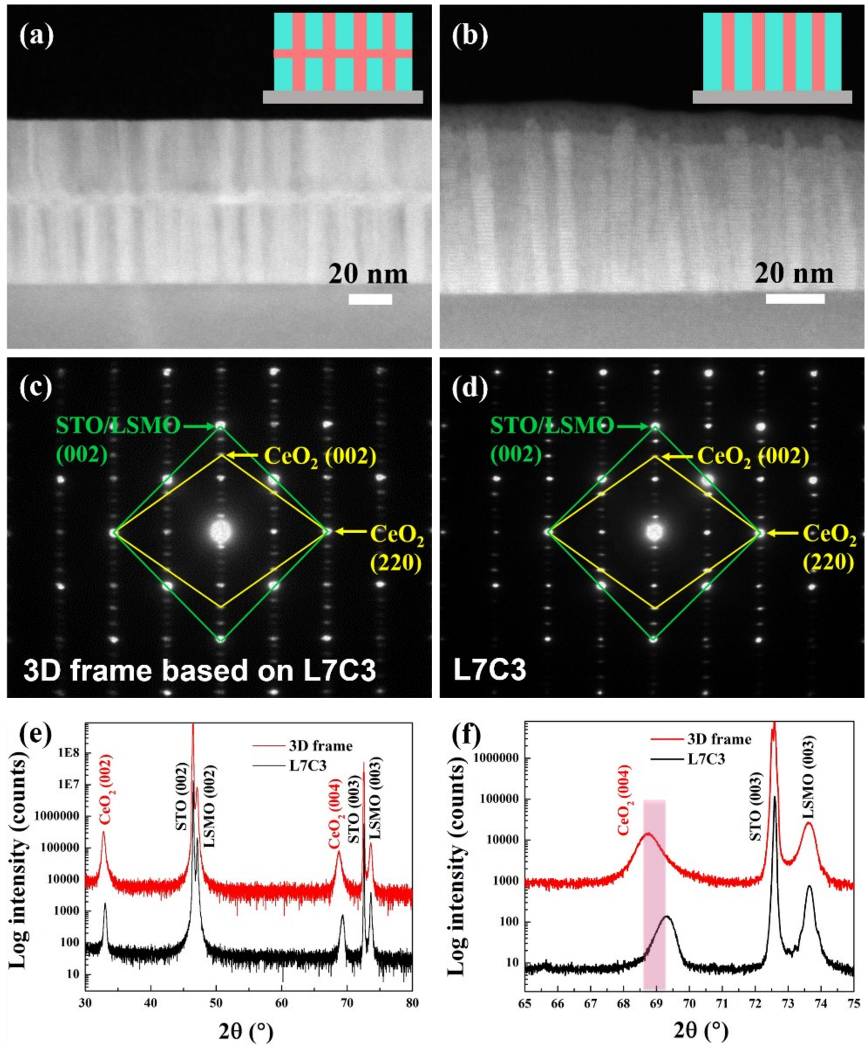

Figure S7. Cross-sectional STEM images of (a) the 3D CeO_2 framed thin film with L7C3 (molar ratio of LSMO:CeO_2 = 7:3) VAN and (b) the L7C3 VAN thin film. The corresponding SAED patterns of (c) the 3D CeO_2 framed thin film and (d) the L7C3 thin film. (e) XRD 2θ-ω patterns of the L7C3 and its 3D CeO_2 framed thin films. (f) Local 2θ-ω scans of these two thin films at CeO_2 (004) and LSMO/STO (003) diffractions (the red band is used to mark the peak shift of CeO_2 (004) diffraction between the single layer L7C3 and the 3D framed film).

References

1. A. P. Chen, Z. X. Bi, H. Hazariwala, X. H. Zhang, Q. Su, L. Chen, Q. X. Jia, J. L. MacManus-Driscoll and H. Y. Wang, *Nanotechnology*, 2011, **22**, 6.
2. M. Fan, W. Zhang, F. Khatkhatay, L. Li and H. Wang, *J. Appl. Phys.*, 2015, **118**, 065302.
3. A. P. Chen, Z. X. Bi, Q. X. Jia, J. L. MacManus-Driscoll and H. Y. Wang, *Acta Mater.*, 2013, **61**, 2783-2792.